# Unsupervised clustering of Southern Ocean Argo float temperature profiles

**Daniel C. Jones[1], Harry J. Holt[1,2], Andrew J.S. Meijers[1], Emily Shuckburgh[1]**

[1]British Antarctic Survey, Cambridge, UK
[2]Department of Physics, University of Cambridge, Cambridge, UK

**Key Points:**

- We apply Gaussian mixture modeling (GMM) to Southern Ocean temperature data
- GMM identifies spatially coherent profile types without using latitude or longitude information
- GMM offers a complementary approach for comparing observational and model datasets

Corresponding author: D. C. Jones, `dannes@bas.ac.uk`

## Abstract

The Southern Ocean has a complex density structure characterized by sharp fronts, steeply tilted isopycnals, and deep seasonal mixed layers. Methods of defining Southern Ocean density structures traditionally rely on somewhat ad-hoc combinations of physical, chemical, and dynamic properties. As an alternative approach, here we apply an unsupervised classification technique (that is, Gaussian mixture modelling or GMM) to Southern Ocean Argo float temperature profiles. GMM, without using any latitude or longitude information, automatically identifies several circumpolar classes influenced by the Antarctic Circumpolar Current. In addition, GMM identifies classes that bear the imprint of mode/intermediate water formation and export, large-scale gyre circulation, and the Agulhas Current. Because GMM is robust, standardized, and automated, it can be used to identify structures in both observational and model datasets, making it a useful complement to existing classification techniques.


## 1 Introduction

The Southern Ocean is a critical component of Earth's climate system, having thus far absorbed greater than 75% of the energy added via anthropogenic emissions and 50% of the excess carbon [*Fletcher et al.*, 2006; *Frölicher et al.*, 2015]. Its ability to absorb heat and carbon comes in part from its unique density structure and circulation, which features upwelling of cold, nutrient rich waters and regions of dense water formation [*Lumpkin and Speer*, 2007]. Characterizing and understanding the mean state and variability of Southern Ocean density structure remains an important and climatically-relevant goal of modern oceanography.

Through decades of effort, the oceanographic community has converged on a description of ocean structure that uses temperature, salinity, dynamical, and biogeochemical patterns to define different water masses (e.g. using potential vorticity minima to locate mode water pools) [*Talley*, 2013, and references therein]. This scheme exploits the understanding that water mass properties are “set" in their formation regions and modified by advection, mixing, and biogeochemical processes. This modern classification scheme is extremely useful and will continue to be useful well into the future, but it is not necessarily ideal for every application. Many of the temperature, salinity, and density values used to delimit one water mass from another are somewhat ad-hoc and very specific (e.g. boundaries between different types of mode water). These schemes are useful for observational data analysis but difficult to apply to numerical models of the ocean, which do not necessarily feature exactly the same structure as the observed ocean [*Sallée et al.*, 2013]. It is therefore prudent to develop and test alternative methods for the classification of different oceanic temperature, salinity, and density structures, as a complement to existing expertise-driven methods.

*Maze et al.* [2017] have shown that Argo profile data from the North Atlantic Ocean can be usefully grouped into classes using Gaussian mixture modelling (GMM), an unsupervised classification technique. GMM describes the spatial structure of Argo profiles by as a collection of Gaussian models whose means and standard deviations generally vary with depth. In this work, we apply GMM to Southern Ocean Argo data in the upper 1000 m of the water column. We find that GMM identifies several circumpolar classes, gyres, salt stratified regions, the Agulhas current, and pathways broadly associated with the formation and export of mode and intermediate waters. In addition, GMM identifies fronts as boundaries between classes and may thus present an alternative method for front location and analysis. In section 2 we describe the Argo dataset and the basics of GMM. In section 3, we present the results of applying GMM to Southern Ocean Argo data, and in seciton 4 we summarize our conclusions.

## 2 Methods

We applied an unsupervised classification method (i.e. Gaussian mixture modelling, hereafter GMM) to Southern Ocean Argo float data. In this section, we briefly describe the Argo dataset and the basics of GMM. We use the scikit-learn machine learning library for Python (`http://scikit-learn.org/`), and the source code used for much of the analysis in this paper is available via Github (`https://github.com/DanJonesOcean/OceanClustering`). We refer the reader to *Maze et al.* [2017] for further detail on applying GMM to Argo float data.

### 2.1 Argo float dataset

Argo floats are autonomous ocean instruments that measure, at minimum, the temperature and salinity of the ocean by periodically taking vertical profiles. Every 10 days, starting at a “neutral" position of 1000 m, an Argo float dives down to 2000 m before rising to the surface, taking a vertical profile of the water column along the way. The measurements are transmitted via satellite and are ultimately made freely available via the Argo Global Data Assembly Centers (GDACs) after some quality control checks. At the time of this writing, over 3800 Argo floats are active in the global ocean, producing over 100,000 temperature and salinity profiles per year with an average spacing of 3° (`http://www.argo.ucsd.edu/`).

For this study, we selected all available Argo profiles south of 30°S that have been flagged by the GDACs as "observation good" (i.e. quality control flag = 1) covering the time period from 2001 to early 2016. More specifically, we used a vertically interpolated product with 400 pressure/depth levels ranging from 0 to 2000 dbar. After discarding profiles with $>= $ 6% NaN values (2% of the initial number of profiles) and discarding depth levels with $>= $ 3% NaN values, we were left with 284,427 profiles, each with 192 pressure levels between 15 dbar and 980 dbar. We replaced all remaining NaN values ($\ll$ 1% of the total temperature measurements) with linearly interpolated estimates using nearest neighbor values. We refer to the resulting dataset as the "cleaned" dataset.

Because of the autonomous and free-drifting nature of the floats, the profiles are not distributed evenly in latitude/longitude (Figure 1). The profiles are more heavily concentrated in the Pacific sector (roughly 890 profiles per degree longitude, totalling 47% of profiles) and Indian sector (800 profiles per degree longitude, totalling 34% of profiles), with relatively fewer profiles in the Atlantic sector (610 profiles per degree longitude, 19% of total). When counted in equal-area bins and plotted by latitude, we see that the number or profiles decreases towards Antarctica (Figure 1(b)), which is partly due to challenging operational conditions associated with seasonal sea ice, which can extend to just north of 60°S at maximum areal extent. The profiles are slightly over-represented in the Austral summer and autumn (DJF-MAM, 52% of profiles) and under-represented in the Austral winter and spring (JJA-SON, 48% of profiles), and the number of profiles increases until 2013 (Figure 1(c,d)). The relatively low number of profiles used in 2016 reflects the time when the particular dataset chosen for this study was generated and does not reflect a lack of profiles in the total Argo dataset.

The profiles selected for this study display a large variety of vertical temperature structures (Figure 2). The range of temperatures is much larger in the surface and considerably narrower at depth, in part reflecting the seasonal cycle in upper ocean temperatures. A large number of profiles feature colder temperatures near the surface and warmer temperatures in the interior, which on its own is physically unstable to convection. However, water masses around Antarctica tend to be fresher at the surface and saltier in the interior due to glacial melt, freshwater flux, and the balance of evaporation/precipitation. This arrangement of tem-

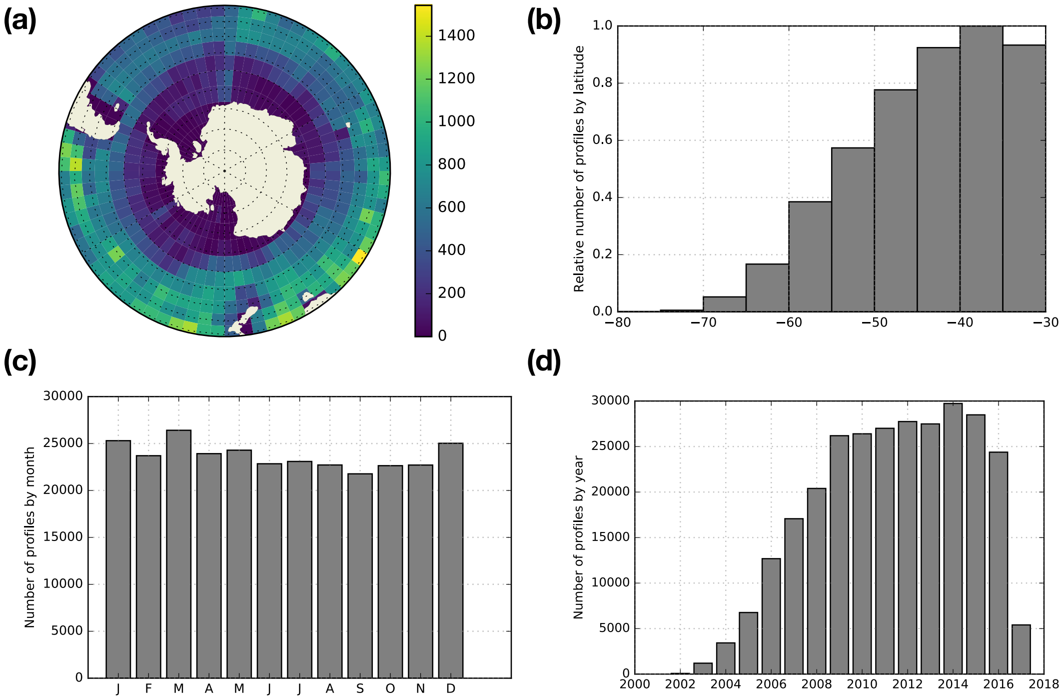


**Figure 1.** Distribution of Argo profiles from the cleaned dataset. (a) Number of profiles in $5^\circ \times 5^\circ$ bins. (b) Relative number of profiles by latitude, scaled by an area-weighting factor $\cos(\phi)$, where $\phi$ is the latitude. The temporal distribution of profiles shown by (c) month and (d) year.

perature and salinity can be stable to vertical mixing (called "salt stratification"). In addition, the thermocline, i.e. the region of the ocean that features a rapid change in temperature with depth, is visible in some temperature profiles.

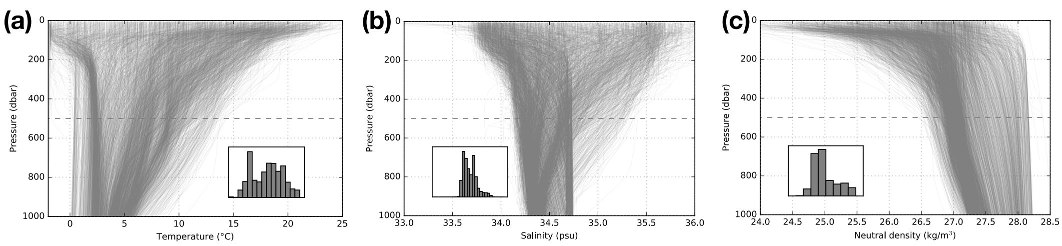


**Figure 2.** Histogram of Argo (a) temperature profiles and (b) salinity profiles in the cleaned dataset. Neural density profiles (c) are derived from temperature and salinity. Only 10% of the profiles are shown for visibility, and pressure levels below 1000 dbar were discarded. Only temperature is used in the clustering analysis.

## 2.2 Gaussian mixture modeling

Gaussian mixture modeling (GMM) is a probabilistic approach to describing and classifying data. It attempts to fit (or “model") the data as a linear combination of multi-dimensional Gaussian distributions with unknown means and unknown standard deviations. Let $\mathbf{X}$ be the array of $N$ vertical profiles, each with $D$ pressure/depth levels, and let $p(\mathbf{X})$ be the probability distribution function (PDF) representing the entire dataset. GMM represents the PDF as a weighted sum of $k$ Gaussian classes, indexed by $c$, i.e.:

$$p(\mathbf{X}) = \sum_{c=1}^{k} \lambda_c \mathcal{N}(\mathbf{X}; \mu_c, \Sigma_c). \tag{1}$$

Here, $k$ is the total number of Gaussian distributions/classes used in the model and $\mathcal{N}(\mathbf{x}; \mu_c, \Sigma_c)$ is the multi-dimensional Gaussian (i.e. normal) PDF with a vector of means $\mu_{\mathbf{c}}$ and covariance matrix $\Sigma_{\mathbf{c}}$, i.e.:

$$\mathcal{N}(\mathbf{x}; \mu_c, \Sigma_c) = \frac{\exp\left[-\frac{1}{2}(\mathbf{x}-\mu_c)^T \Sigma_c^{-1} (\mathbf{x}-\mu_c)\right]}{\sqrt{(2\pi)^D \left|\Sigma_c\right|}}. \tag{2}$$

The probability associated with class/component $c_a$ is $p(c = c_a) = \lambda_{c_a}$. The probability of profile $\mathbf{x}$ being in class/component $c_a$ is $p(\mathbf{x}|c = c_a) = \mathcal{N}(\mathbf{X}; \mu_{c_a}, \sigma_{c_a})$, where the vector $\mathbf{x}$ is a single profile taken from the complete array $\mathbf{X}$. Both $\mathbf{x}$ and $\mu_{\mathbf{c}}$ are vectors of length $D$.

Starting with random initial guesses for the classes, GMM proceeds by iteratively adjusting the means $\mu_{\mathbf{c}}$ and standard deviations $\Sigma_{\mathbf{c}}$ (i.e. the “parameters") of the classes in order to maximize a logarithmic measure of likelihood, i.e.:

$$\log[p(\mathbf{X})] = \sum_i \log\left[\sum_{c=1}^{k} \lambda_c \mathcal{N}(\mathbf{X}; \mu_c, \Sigma_c)\right], \tag{3}$$

It does so following an expectation-maximization approach, described in *Maze et al.* [2017]. This algorithm monotonically converges on a local maximum. GMM is a generalization of $k$-means clustering, which only attempts to minimize in-group variance by shifting the means. By contrast, GMM attempts to identify means and standard deviations, allowing for some variation about the centres of the Gaussian distributions.

In our instance of GMM, each depth level is treated as a “dimension" with Gaussian parameters associated with each depth level. However, we may not need all of these depth levels to accurately describe the dataset, as ocean temperature changes much more rapidly in the mixed layer and thermocline than in the interior. In order to reduce the computational complexity of the problem, we transform the profile data from pressure/depth space to an alternative space using principal component analysis (PCA). Specifically, we calculate principal components that capture a desired fraction of the vertical variability of the dataset. Each eigenvector may be thought of as a "profile type" that describes a certain amount of variance in the data with depth (note that this is not necessarily the same thing as a "typical profile"). We calculate $d$ principal components and employ the transformation:

$$\mathbf{X}(z) = \sum_{j=1}^{d} \mathbf{P}(z, j)\mathbf{Y}(j), \tag{4}$$

where $z$ is the depth level, $d$ is the total number of principal components (index $j$), and $\mathbf{P}(z, j)$ is the transformation matrix between pressure/depth space and principal component space. We find that $d = 6$ captures 99.9% of the variance in the vertical structure, which greatly reduces the number of dimensions needed to describe the Argo profile data used here, i.e. from 194 pressure/depth levels to 6 principal components.

GMM does have one free parameter, i.e. the maximum number of classes $k$. In order to determine the most appropriate value for $k$, we applied two statistical tests, namely (i) a Bayesian Information Criterion (BIC) and (ii) a Variational Bayesian GMM (VB-GMM) test. The first test (BIC) uses an empirically formulated cost function that rewards likelihood and penalizes the number of classes $k$:

$$BIC(k) = -2\mathcal{L}(k) + N_f(k)\log(n), \tag{5}$$

where $\mathcal{L}$ is a measure of likelihood, $n$ is the number of profiles used in the BIC test, and $N_f$ is the number of independent parameters to be estimated:

$$N_f(k) = k - 1 + kD + \frac{kD(D-1)}{2}. \tag{6}$$

The decorrelation scale in the Southern Ocean is approximately 300 km [*Ninove et al.*, 2016]. Using this 300 km scale as guidance, we randomly select a profile from each $4° \times 4°$ grid cell, returning 884 random profiles for each BIC test. We calculate BIC scores for each set of 884 random profiles (in principal component space) using a range of classes $k$ from 1 to 19 (Figure 3(a)). Although BIC does not return a clear, single minimizer $k_{min}$, it suggests that the optimum $k_{min}$ value lies between 6 and 10.

As a complement to BIC, we also used VB-GMM to determine the optimum number of classes $k$, available as a function within scikit-learn. This clustering method assigns a weight to each class. Based on this test, we choose $k = 8$, as higher values of $k$ fall below the level of equal probability (0.05 for 20 classes) (Figure 3(b)). In addition, our choice of $k = 8$ is partly informed by the value that returns a physically useful description of ocean structure.

Clustering algorithms organise data into groups or sets according to a defined rule, ideally identifying structures in the dataset. Oceanography has a rich history of expertise-driven

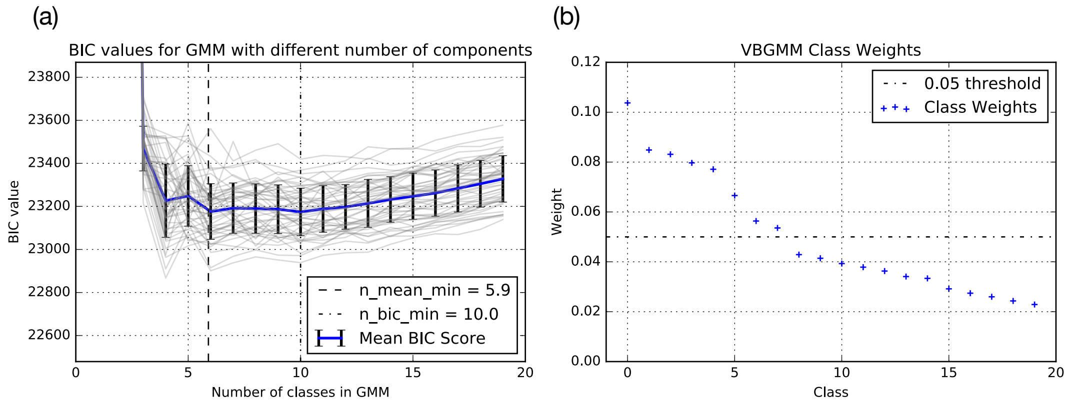


**Figure 3.** (a) Bayesian Information Criteria (BIC) scores versus the specified number of classes $k$. Shown are the individual trials for different subsets of the temperature profile datasets (grey lines), the mean (blue line), and standard deviations computed from the profiles. The dashed line represents the average of the minimums from each profile and the dash-dot line represents the minimum of the average of the profiles. (b) Class weights from VB-GMM with up to 20 components, indexed from 0 to 19. The dash-dot line is a line of equal probability for 20 classes 0.05.

clustering using physical and biogeochemical criteria (e.g. PV minima, oxygen minima), fingerprints of physical and biogeochemical processes, and identifiable patterns. These descriptions can be arranged into hierarchies, from coarse/simple (e.g. two-layer quasi-geostrophic models) to rich and complex (e.g. the descriptions found in *Talley* [2013]). The level of detail required in the description depends on the application at hand. For example, a simple $\beta$-plane model is sufficient to explain the existence of gyres and western boundary currents; it constitutes a first-order description of gyres. Algorithmic clustering offers a robust way to traverse this hierarchy. As we have seen, BIC and VB-GMM suggest that the optimum number of classes is between 6 and 10. Although these statistical tests can be used as a rough guide for choosing the number of classes, there is not necessarily a single “correct/ideal" value for $k$, which can be thought of as a weakly constrained parameter indicating the level of complexity in the statistical description of the dataset. We explore the impact of $k$ on our results in the appendix.

Below we refer to “training" datasets and “test" datasets. Both are subsets of the cleaned dataset. BIC and GMM generally use different training datasets. For the GMM training set, we randomly selected a single profile from each $1^\circ \times 1^\circ$ bin. Each training dataset contains 12,286 profiles (roughly 4% of the cleaned dataset), distributed evenly in latitude/longitude space. We use the training dataset to estimate the parameters (i.e. the means and standard deviations) of the GMM classes, and then we statistically represent (i.e. 'model') the test dataset with the fitted Gaussian model with optimized parameters. The end result is a probabilistic description of the cleaned Argo dataset in terms of a linear combination of Gaussian distributions that vary with depth.

## 3 Results

We describe the cleaned Argo temperature profiles as a linear combination of multi-dimensional Gaussian functions in order to identify patterns in the temperature structure of the Southern Ocean. As an initial test, we start with a simple one-dimensional case by clustering vertical mean temperatures. The GMM algorithm identifies spatially-coherent patterns, despite not having access to the longitudes or latitudes of the profiles (Figure 4). On the basin-scale, GMM identifies patterns that roughly correspond to some physically familiar temperature structures. For instance, there are several circumpolar classes (labeled 0, 3, and 7), consistent with the tendency of the Antarctic Circumpolar Current (ACC) to homogenize properties along its streamlines. The circumpolar class closest to Antarctica (class 7) also extends throughout the Weddell Gyre. Having shown that GMM can identify spatially coherent structures without using latitude/longitude data, we turn our attention to vertical variations in temperature.

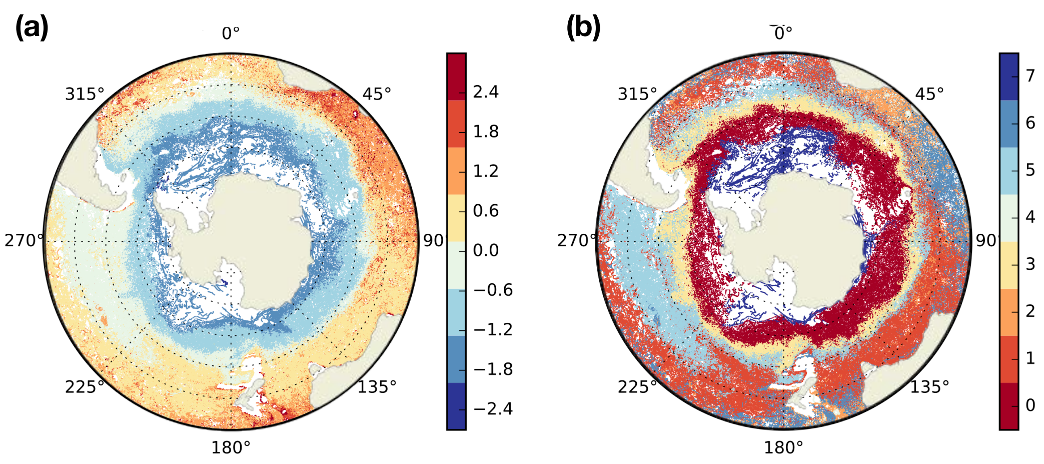


**Figure 4.** (a) Vertically averaged temperature anomaly (°C) relative to the domain mean. (b) GMM classes for vertical mean temperature, calculated with $k = 8$. Indexing starts with zero.

We classify Argo profiles from our “cleaned" dataset into $k = 8$ different clusters, and as with the vertical mean temperature case, we find spatially coherent structures (Figure 5). The class nearest Antarctica (class 7) extends throughout the Weddell Gyre and around coastal Antarctica. The mean profiles in this region tend to be salt stratified. The near-Antarctic class coincides with regions of deep water formation and upwelling of dense water, and its northern boundary coincides with the classical “southern boundary" front (SBDY) of the Antarctic Circumpolar Current [*Orsi et al.*, 1995]. This class occupies a narrow range in dynamic height space and is fairly distinct from the other classes (i.e. profiles of this class type are very rarely found north of the classical southern boundary), indicating that GMM has identified a cluster that is physically distinct and identifiable.

North of the SBDY, GMM identifies two circumpolar classes (classes 1 and 3). The southernmost circumpolar class (class 1) is located south of the Polar Front (PF) and is consistent with the homogenizing tendency of ACC circulation. The second circumpolar class (class 3) is mostly located south of the classical SAF. As with the near-Antarctic class, classes 1 and 7 occupy distinct regions when plotted in dynamic height space at all longitudes, indicating that they are indeed physically separate from the others. Class 0 is located just north of the SAF in the Pacific and Indian sectors. Together with the Pacific component of class 5, these two clusters roughly coincide with broad patterns associated with the formation and export of Subantarctic Mode Water and Antarctic Intermediate Water, both of which may impact the temperature structure of the local water column [*Iudicone et al.*, 2007; *Jones et al.*, 2016]. Similarly, class 2 is spatially coincident with the westward export pathway of mode water formed in the deep mixed layers south of Australia [*Jones et al.*, 2016, Fig. 4b]. GMM identifies a class that overlaps with the Agulhas current and retroflection (class 6), although in dynamic height space this class overlaps with others. Profiles in class 6 are also found east of New Zealand. Class 4 is associated with subtropical water and represents the lowest-latitude profiles in the Atlantic and Pacific basins.

In order to classify the Argo profiles based on their vertical structures, we applied GMM to the centered, standardized training dataset in principal component (PC) space. Although direct physical interpretation of the fits in PC space is difficult, we see that the $k = 8$ component Gaussian distribution is able to capture the broad features of the values associated with each principal component (Figure 6). The Gaussians are more distinct and spread out for the first three principal components, whereas the higher indexed PCs feature more overlap between Gaussian classes.

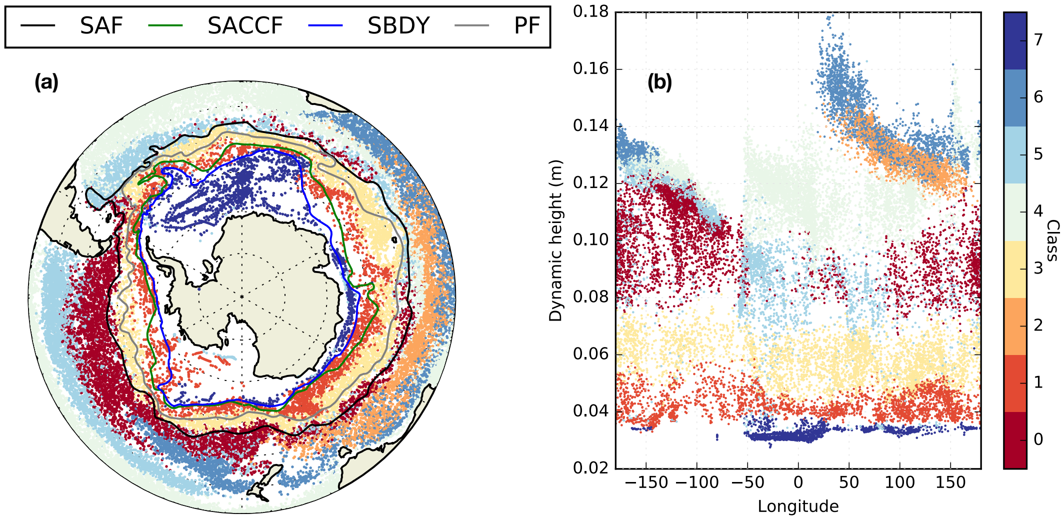


**Figure 5.** (a) GMM-derived class distribution for $k = 8$, shown with four fronts of the Antarctic Circumpolar Current, i.e. the Subantarctic Front (SAF), Southern ACC Front (SACCF), Southern Boundary (SBDY), and the Polar Front (PF) [*Orsi et al.*, 1995]. (b) Class distribution shown in dynamic height space. Note that only points with posterior probability ≥ 0.9 are shown.

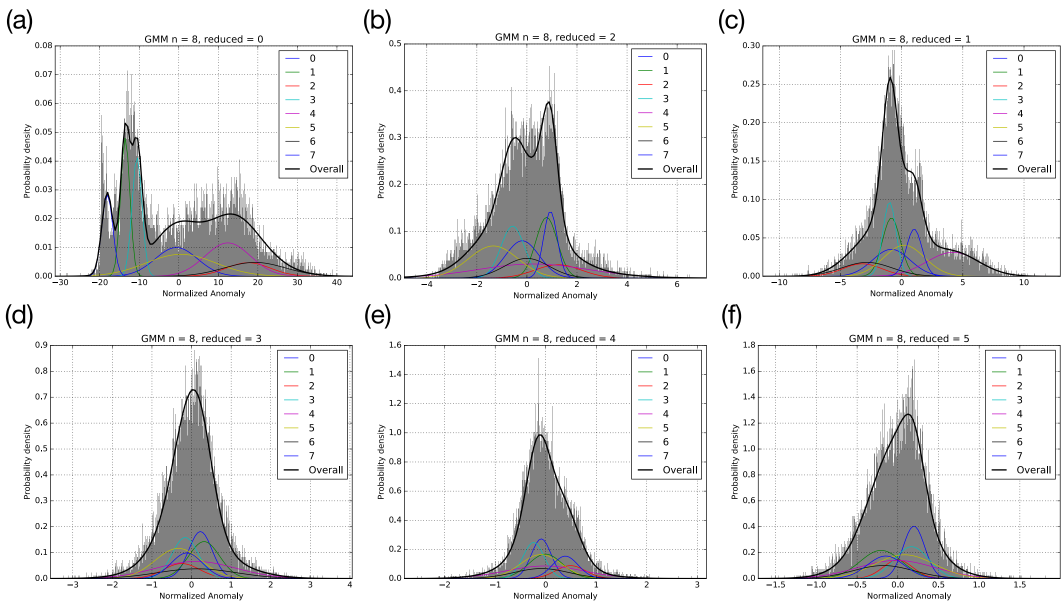


**Figure 6.** Probability density functions for each principal component (referred to as "reduced depth levels" in the plot). For each principal component, each Gaussian component is shown.

The mean temperature profiles associated with each class show several different types of vertical temperature profiles (Figure 7). We see three inverted profiles that are cooler near the surface and warmer with depth. These correspond to salt stratified profiles, i.e. where the vertical stability of the profile relies on the salt distribution, which is necessarily a fresh surface layer overlying a denser, saltier interior. Many of these profiles can be found in the Weddell Sea and near the wider Antarctic shelf. Other classes feature a decrease in temperature from the surface into the interior, with different means and vertical structures.

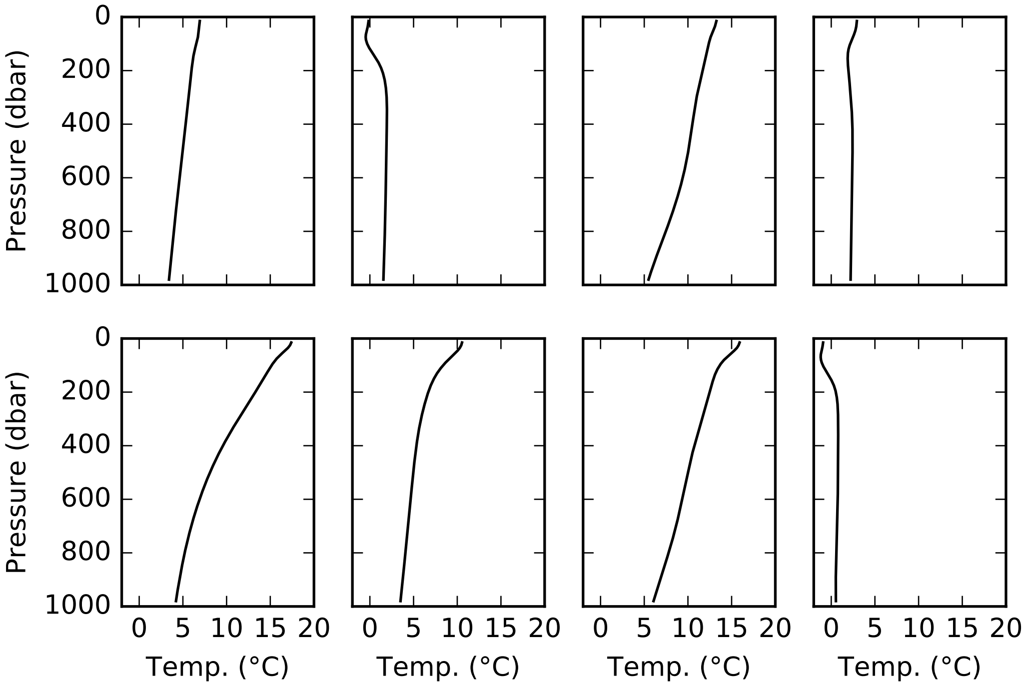


**Figure 7.** GMM class mean temperature profiles with depth.

One advantage of GMM over k-means clustering is that GMM returns posterior probabilities, i.e. measures of the likelihood of each class assignment (Figure 8). On basin scales, the posterior probabilities associated with each of the 8 classes is above 0.8, which quantifies the likelihood that the classes have been assigned to the most suitable class. Many of the regions in which the posterior probabilities are low correspond to regions of strong mixing, although low sampling may affect the probabilities as well. We also find probabilities less than 0.8 at the boundaries between classes, indicating the degree of relative smoothness of transitions between different class types.

## 4 Conclusions

We applied Gaussian Mixture Modeling (GMM), an unsupervised classification scheme, to Southern Ocean Argo float data above 1000 m. Without using longitude or latitude infor-

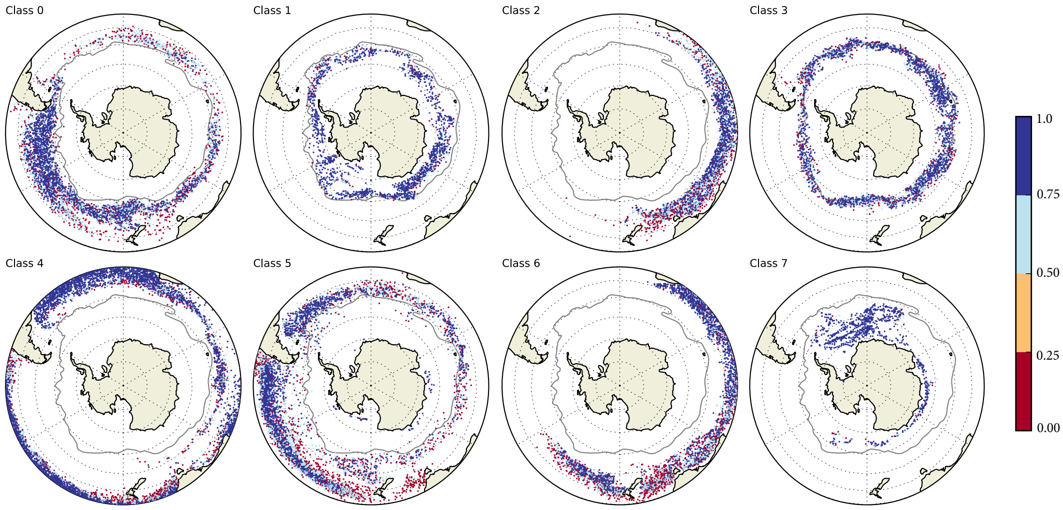


**Figure 8.** Posterior probabilities for the 8 classes, shown together with the Polar Front of the ACC.

mation, GMM identified spatially coherent patterns in the vertical temperature structure. The GMM-derived classes broadly coincide with large-scale circulation and stratification features, including regions of bottom water formation and upwelling (i.e. adjacent to Antarctica), the Antarctic Circumpolar Current, formation and export pathways of Subantarctic Mode Water and Antarctic Intermediate Water, subtropical gyre circulation, and the Agulhas Current and associated retroflection. The class boundaries broadly coincide with several classically-defined fronts of the ACC, and the circumpolar classes occupy distinct regions in dynamic height space, indicating that GMM has identified physically distinct profile types using only vertical temperature data. Posterior probability distributions indicate regions where the classes are distinct and statistically separate, whereas regions with low posterior probability indicate boundaries between classes and/or regions of mixing influenced by a number of different temperature structures. GMM offers an alternative, complementary method for classification of Southern Ocean density structures, and it is potentially useful for objectively and automatically comparing structures across different observational and modeling datasets.

## A: Sensitivity to number of classes $k$

In this work, the number of classes $k$ is constrained between 6 and 10. This weak constraint allows for some tuning depending on the desired level of complexity in the description of the dataset. Using $k = 6$ classes is sufficient to capture most of the large-scale structures identified in the $k = 8$ case, except that (1) the cluster found in the Agulhas retroflection region and in the area east of New Zealand (class 5 for $k = 8$) is grouped together with the Indian-Australian cluster that is spatially coincident with mode water formation and export (class 3 for $k = 6$) and (2) the cluster in the Pacific that spatially coincides with a region of mode water formation and export (classes 0 and 6 for $k = 8$) only contains one class instead of two (class 2 for $k = 6$). Moving from $k = 8$ to $k = 12$, several classes get split into smaller clusters, e.g. the class overlapping the Pacific mode waters splits into eastward and westward components, the class south of Australia splits into northern/southern components (Figure A.1(c)). The Weddell Sea class is identifiable for $k$ between 6 and 12. The number of circumpolar classes on and south of the Polar Front increases from 2 to 3 as we increase $k$ from 8 to 12. Values of $k$ much smaller than 6 or much larger than 12 lose many of the characteristic fingerprints of the large-scale circulation processes discussed here (e.g. the along-streamline homogenization enforced by the circulation of the ACC).

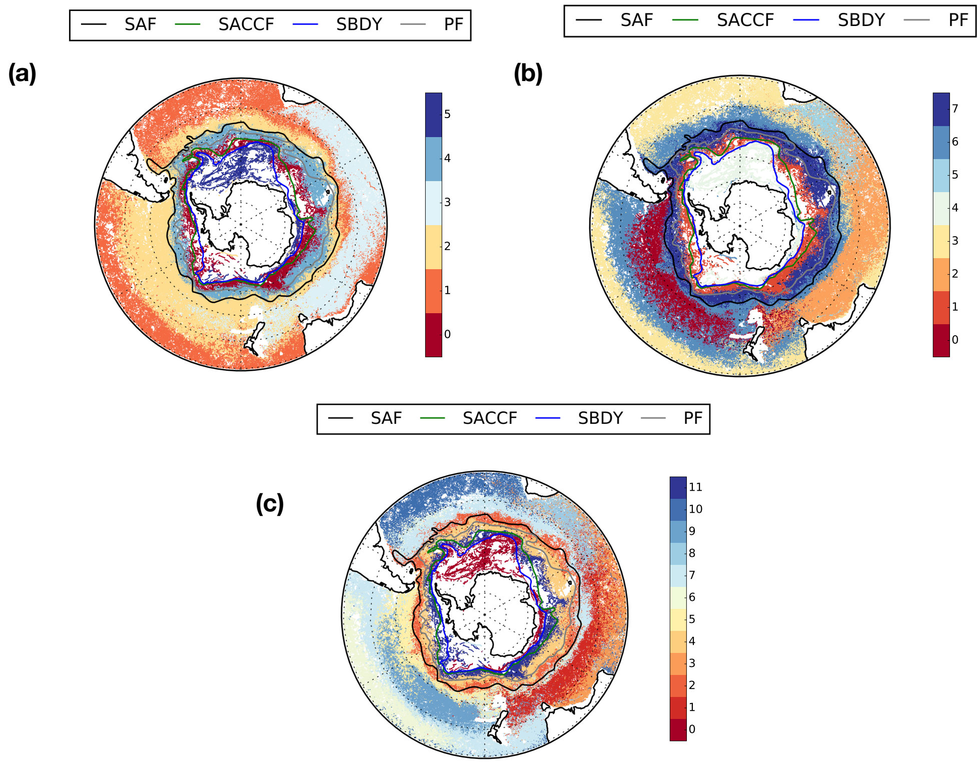


**Figure A.1.** Comparison of GMM-derived classes, shown for (a) 6 classes, (b) 8 classes, and (c) 12 classes. Also shown are classically-defined fronts of the Antarctic Circumpolar Current.

## Acronyms

**AAIW** Antarctic Intermediate Water

**ACC** Antarctic Circumpolar Current

**ARGO** Array for Real-time Geostrophic Oceanography

**BIC** Bayesian Information Criterion

**GDAC** Global Data Assembly Center

**GMM** Gaussian mixture modeling

**PCA** Principal component analysis

**PDF** Probability distribution function

**SAMW** Subantarctic Mode Water

**VB-GMM** Variational Bayesian Gaussian mixture modelling

## Acknowledgments

This study is supported by grants from the Natural Environment Research Council (NERC), including [1] The North Atlantic Climate System Integrated Study (ACSIS) [grant NE/N018028/1 (authors DJ, ES)] and [3] Ocean Regulation of Climate by Heat and Carbon Sequestration and Transports (ORCHESTRA) [grant NE/N018095/1 (authors ES, AM)]. HH was funded by a NERC DTP Research Experience Placement over the summer of 2017 [grant NE/L002434/1]. Argo float data is freely available for download at `http://www.argo.ucsd.edu/`. The analysis software used in this manuscript was written using Python and the scikit-learn machine learning library (`http://scikit-learn.org/stable/`). The scripts we used are available via github (`https://github.com/DanJonesOcean/OceanClustering`). DJ thanks Chris Lowder for python support. We are grateful to J.-B. Sallée for front data for the Antarctic Circumpolar Current.

## References

Fletcher, S. E. M., N. Gruber, A. R. Jacobson, S. C. Doney, S. Dutkiewicz, M. Gerber, M. Follows, F. Joos, K. Lindsay, D. Menemenlis, A. Mouchet, S. A. Müller, and J. L. Sarmiento (2006), Inverse estimates of anthropogenic CO2 uptake, transport, and storage by the ocean, *Global Biogeochemical Cycles*, *20*(2), doi:10.1029/2005gb002530.

Frölicher, T. L., J. L. Sarmiento, D. J. Paynter, J. P. Dunne, J. P. Krasting, and M. Winton (2015), Dominance of the Southern Ocean in Anthropogenic Carbon and Heat Uptake in CMIP5 Models, *Journal of Climate*, *28*(2), 862–886, doi:10.1175/jcli-d-14-00117.1.

Iudicone, D., K. Rodgers, R. Schopp, and G. Madec (2007), An exchange window for the injection of Antarctic Intermediate Water into the South Pacific, *Journal of Physical Oceanography*, *37*, 31–49, doi:http://dx.doi.org/10.1175/JPO2985.1.

Jones, D. C., A. J. S. Meijers, E. Shuckburgh, J.-B. Sallée, P. Haynes, E. K. McAufield, and M. R. Mazloff (2016), How does Subantarctic Mode Water ventilate the Southern Hemisphere subtropics?, *Journal of Geophysical Research - Oceans*, *121*(9), 6558–6582, doi:10.1002/2016jc011680.

Lumpkin, R., and K. Speer (2007), Global ocean meridional overturning, *Journal of Physical Oceanography*, *37*, 2550–2562, doi:10.1175/JPO3130.1.

Maze, G., H. Mercier, R. Fablet, P. Tandeo, M. L. Radcenco, P. Lenca, C. Feucher, and C. Le Goff (2017), Coherent heat patterns revealed by unsupervised classification of Argo temperature profiles in the North Atlantic Ocean, *Progress in Oceanography*, *151*, 275–292, doi:10.1016/j.pocean.2016.12.008.

Ninove, F., P. Y. Le Traon, E. Remy, and S. Guinehut (2016), Spatial scales of temperature and salinity variability estimated from Argo observations, *Ocean Science*, *12*(1), 1–7, doi:10.5194/os-12-1-2016.

Orsi, A., T. Whitworth, and W. Nowlin (1995), On the meridional extent and fronts of the Antarctic Circumpolar Current, *Deep Sea Research Part I*, *42*(5), 641–673.

Sallée, J., E. Shuckburgh, N. Bruneau, A. Meijers, T. Bracegirdle, Z. Wang, and T. Roy (2013), Assessment of Southern Ocean water mass circulation and characteristics in CMIP5 models: historical bias and forcing response, *Journal of Research: Oceans*, *118*, 1830–1844, doi:10.1002/jgrc.20135.

Talley, L. (2013), Closure of the Global Overturning Circulation Through the Indian, Pacific, and Southern Oceans: Schematics and Transports, *Oceanography*, *26*(1), 80–97, doi:10.5670/oceanog.2013.07.